Electronic Supplementary Information

Formation of a long-lived radical pair in a Sn(IV) porphyrin-di(L-tyrosinato) conjugate driven by proton-coupled electron-transfer

Mirco Natali,[a]* Agnese Amati,[b] Nicola Demitri,[c] Elisabetta Iengo[b]*

[a] Department of Chemical and Pharmaceutical Sciences, University of Ferrara, and Centro Interuniversitario per la Conversione Chimica dell'Energia Solare (SolarChem), sez. di Ferrara, via L. Borsari 46, 44121 Ferrara, Italy.

E-mail: mirco.natali@unife.it

[b] Department of Chemical and Pharmaceutical Sciences, University of Trieste, Via L. Giorgieri 1, 34127, Trieste, Italy.

E-mail: eiengo@units.it

[c] Elettra – Sincrotrone Trieste, S.S. 14 Km 163.5 in Area Science Park, 34149 Basovizza – Trieste, Italy.

Table of content

S1. Experimental section

Materials. Chemicals were purchased from Sigma-Aldrich or Alfa Aesar and used without further purification, unless otherwise stated. Solvents for spectroscopic measurements were of spectroscopic grade, all other chemicals were of reagent grade quality, and used as received. *trans*-dihydroxo(5,10,15,20-tetraphenylporphyrinato)-tin(IV) $SnP(OH)_2$ and *trans*-dibenzoato(5,10,15,20-tetraphenylporphyrinato)-tin(IV), $SnP(BA)_2$ (**2**), were prepared as reported earlier.[S1]

NMR. Mono- and bi-dimensional NMR experiments (^{1}H, H-H COSY, H-C COSY) were recorded on a Varian 500 (500 MHz) spectrometer. All spectra were run at room temperature; ^{1}H and ^{13}C chemical shifts were referenced to the peak of residual non-deuterated solvents: δ (ppm) = 2.5 and δ (ppm) = 39.52, respectively, for dmso-d_6; δ (ppm) = 1.94 for $CDCl_3/CD_3CN$ 5:1.

Mass. Electrospray ionization mass spectrometry (ESI-MS) measurements were performed on a Perkin–Elmer APII spectrometer at 5600 eV by Dr. Fabio Hollan, Department of Chemical and Pharmaceutical Sciences, University of Trieste, Italy.

IR. Infrared spectra were recorded on a Perkin-Elmer FT-IR 2000 spectrometer in the transmission mode and the samples were prepared as KBr pellets.

Circular Dichroism. CD spectra were recorded on a JASCO J-815 CD spectrometer, with a 1 mm optical path quartz cuvette.

Crystal structure determination. Data collections were performed at the X-ray diffraction beamline (XRD1) of the Elettra Synchrotron, Trieste (Italy).[S2] The crystals were dipped in NHV oil (Jena Bioscience, Jena, Germany) and mounted on the goniometer head with kapton loops (MiTeGen, Ithaca, USA). Complete datasets were collected at 100 K (nitrogen stream supplied through an Oxford Cryostream 700 - Oxford Cryosystems Ltd., Oxford, United Kingdom) through the rotating crystal method. Data were acquired using a monochromatic wavelength of 0.700 Å for **1**, on a Pilatus 2M hybrid-pixel area detector (DECTRIS Ltd., Baden-Daettwil, Switzerland). The diffraction data were indexed and integrated using XDS.[S3] Two dataset, collected on the same crystal (randomly oriented),

have been merged and scaled using CCP4-Aimless code.[S4,S5] The structures were solved by the dual space algorithm implemented in SHELXT.[S6] Fourier analysis and refinement were performed by the full-matrix least-squares methods based on F^2 implemented in SHELXL (Version 2017/1).[S6] The Coot program was used for modeling.[S7] Anisotropic thermal motion refinement have been used for all atoms. Hydrogen atoms were included at calculated positions with isotropic $U_{factors} = 1.2\ U_{eq}$ or $U_{factors} = 1.5\ U_{eq}$ for methyl and hydroxyl groups (U_{eq} being the equivalent isotropic thermal factor of the bonded non-hydrogen atoms). One full **1** complex is found in the crystallographic asymmetric unit (ASU, Figure S6). Two ordered acetone molecules have been modeled in crystal cavities. Geometric parameter restrains (SAME AND FLAT) have been applied on solvent molecules. The content of residual voids, filled with disordered solvent molecules have been removed with the SQUEEZE routine of PLATON (99 electrons in 17% - 296 $Å^3$ - of the unit cell volume, split in two similar pockets).[S8] The disordered solvent has been estimated as additional two diethyl ether molecules per cell; contributions of these molecules have been included in the properties reported in Table S1. Refined Flack parameters confirm the expected tyrosine C_α configurations (*S*).[S9] Pictures were prepared using Ortep3[S10] and Pymol[S11] softwares. Selected crystal and refinement data are reported below (Table S1 and Table S2).

Electrochemical Measurements. Cyclic Voltammetry (CV) measurements were carried out with a PC-interfaced *Eco Chemie Autolab/Pgstat 30* Potentiostat. Nitrogen-purged 10^{-3} M sample solutions in dichloromethane, containing 0.1 M $TBAPF_6$ (Tetrabutylammonium hexafluorophosphate, Fluka, electrochemical grade, 99%, dried in an oven), were used. A conventional three-electrode cell assembly was adopted: a saturated calomel electrode (SCE Amel) and a platinum electrode, both separated from test solution by a glass frit, were used as reference and counter (CE) electrodes, respectively; a glassy carbon (GC) electrode was used as the working electrode (WE).

Steady-state Absorption/Emission Measurements. UV-Vis absorption spectra were recorded on both a *Jasco V-570 UV/Vis/NIR* and a *Cary 300 UV-Vis* (*Agilent Technologies*) spectrophotometers. Emission spectra were taken on an *Edinburgh Instrument* spectrofluorimeter equipped with a 900 W

Xe arc lamp as excitation source, a photomultiplier tube, and an InGaAs detector for the visible and the NIR detection, respectively.

Time-Correlated Single Photon Counting (TCSPC). Fluorescence lifetimes were measured using a TC-SPC apparatus (*PicoQuant Picoharp 300*) equipped with subnanosecond LED sources (280, 380, 460, and 600 nm, 500-700 ps pulse width) powered by a *PicoQuant PDL 800-B* variable (2.5-40 MHz) pulsed power supply. The decays were analyzed by means of *PicoQuant FluoFit* Global Fluorescence Decay Analysis Software.

Nanosecond Laser Flash Photolysis. Nanosecond transient measurements were performed with a custom laser spectrometer comprised of a *Continuum Surelite II* Nd:YAG laser (FWHM 6 – 8ns) with frequency doubled, (532 nm, 330 mJ) or tripled, (355 nm, 160 mJ) option, an *Applied Photophysics* xenon light source including a mod. 720 150W lamp housing, a mod. 620 power controlled lamp supply and a mod. 03 –102 arc lamp pulser. Laser excitation was provided at 90° with respect to the white light probe beam. Light transmitted by the sample was focused onto the entrance slit of a 300 mm focal length *Acton SpectraPro 2300i* triple grating, flat field, double exit monochromator equipped with a photomultiplier detector (*Hamamatsu R3896*) and a *Princeton Instruments PIMAX II* gated intensified CCD camera, using a *RB Gen II* intensifier, a ST133 controller and a PTG pulser. Signals from the photomultiplier (kinetic traces) were processed by means of a *TeledyneLeCroy 604Zi* (400 MHz, 20 Gs/s) digital oscilloscope.

Transient measurements were performed on both air-equilibrated samples and oxygen-free solutions, the latter were obtained by purging dichloromethane solutions with nitrogen gas for ca 10 minutes before the experiment.

S2. Synthesis and characterization of *trans*-di(N-acetyl-L-tyrosinato)[5,10,15,20-tetraphenylporphyrinato]-tin(IV), SnP-TyrOH (1)

trans-dihydroxo(5,10,15,20-tetraphenylporphyrinato)-tin(IV), $SnP(OH)_2$, (20.4 mg, 0.027 mmol) was dissolved in 20 mL of $CHCl_3$, and N-acetyl-L-tyrosine (12.5 mg, 0.056 mmol) was then added to the clear violet solution. After having stirred at reflux for 12 hours, the reaction mixture turned to a slightly coloured solution with a purple precipitate. The solvent was removed on a rotary evaporator, the solid was dissolved in 10 mL of $CHCl_3$:acetone 9:1 and *n*-hexane was added to induce the precipitation of pure product as purple crystals (30.2 mg, 0.026 mmol, 95% yield). ^{1}H NMR (500 MHz, dmso-d_6) δ (ppm) 9.22 (s, 8H, Hh), 8.91 (s, 2H, Ha), 8.27 (d, J = 5.4 Hz, 8H, Hi), 7.91 (m, 12H, Hl, Hm), 6.15 (d, J = 7.2 Hz, 4H, Hb), 5.87 (d, J = 7.7 Hz, 2H, Hf), 5.37 (d, J = 7.2 Hz, 4H, Hc), 0.99 (m, 2H, He), 0.86 (s, 6H, Hg), -0.08 (m, 2H, Hd), -0.69 (m, 2H, Hd'); ^{13}C NMR (125 MHz, from HSQC) δ (ppm) 134.31 (Ci), 132.77 (Ch), 128.33 (Cc), 128.70 (Cm), 127.18 (Cl), 114.09 (Cb), 51.92 (Ce), 33.53 (Cd), 21.26 (Cg). ^{1}H NMR (500 MHz, $CDCl_3$/CD_3CN 5:1) δ 9.22 (m, 8H, Hh, ^4J(Sn–H) = 15.2 Hz), 8.21 (d, J = 6.9 Hz, 8H, Hi), 7.81 (m, 12H, Hl, Hm), 6.06 (d, J = 8.3 Hz, 4H, Hb), 4.56 (d, J = 8.3 Hz, 4H, Hc), 3.77 (d, J = 7.1 Hz, 2H, Hf), 1.33 (m, 2H, He), 1.05 (s, 6H, Hg), 0.84 (dd, J = 13.1, 5.5 Hz, 2H, Hd), -0.22 (dd, J = 13.0, 3.9 Hz, 2H, Hd'). Selected IR bands (cm^{-1}, KBr pellets): 3422 ($\tilde{\upsilon}_{OH}$), 1646 ($\tilde{\upsilon}_{C=O}$). UV–Vis (λ_{max}, nm, CH_2Cl_2): 403, 421, 518, 558, 596. ESI-MS (*m*/*z*) (positive mode) for $C_{55}H_{40}N_5O_4Sn_1$ [**1** − one tyrosinato]$^+$ 954.2, found 954.2.

Single crystals suitable for X-ray diffraction were obtained by slow diffusion of diethyl ether over a concentrated solution of **1** in $CHCl_3$:acetone 9:1.

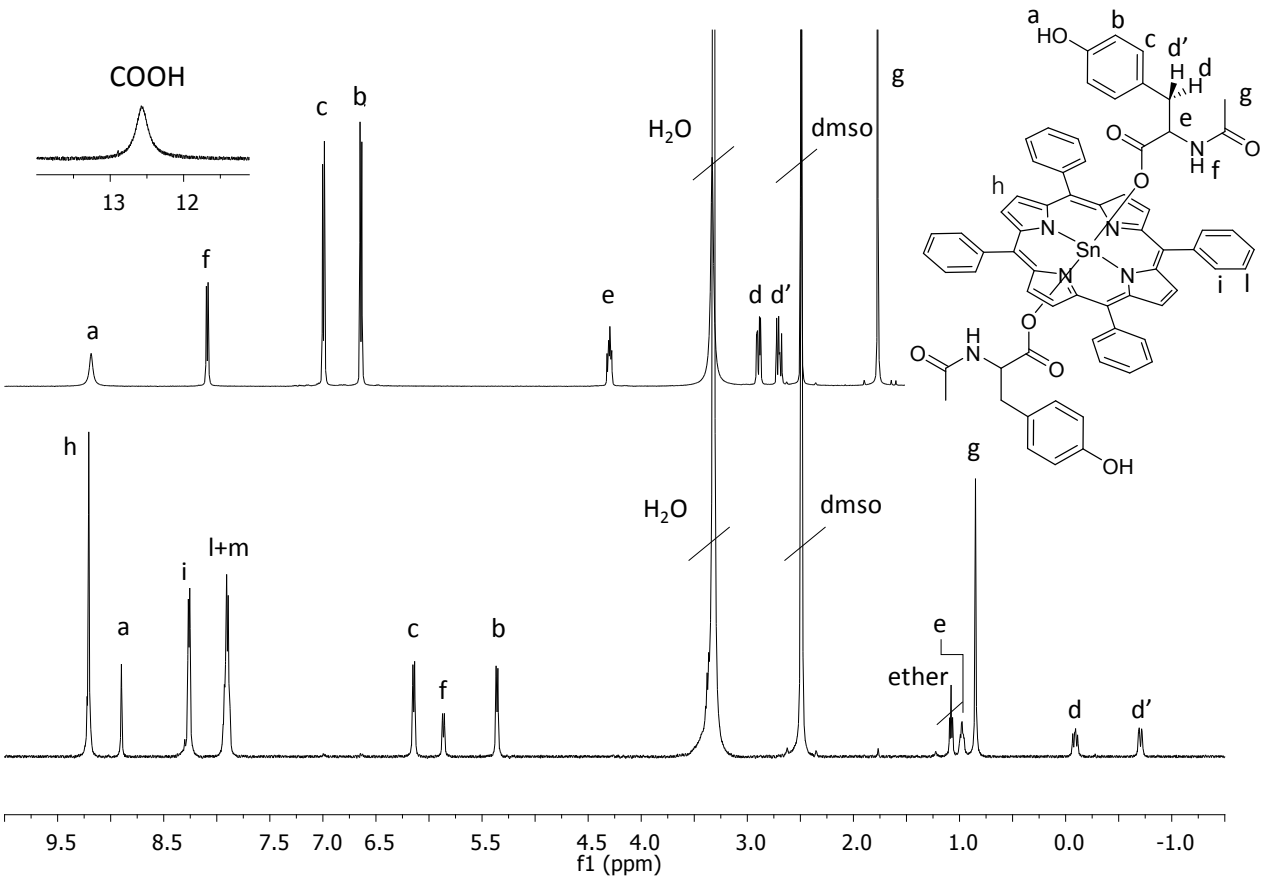

Figure S1. ^{1}H NMR spectra (dmso-d_6) of N-acetyl-L-tyrosine (top) and **1** (bottom).

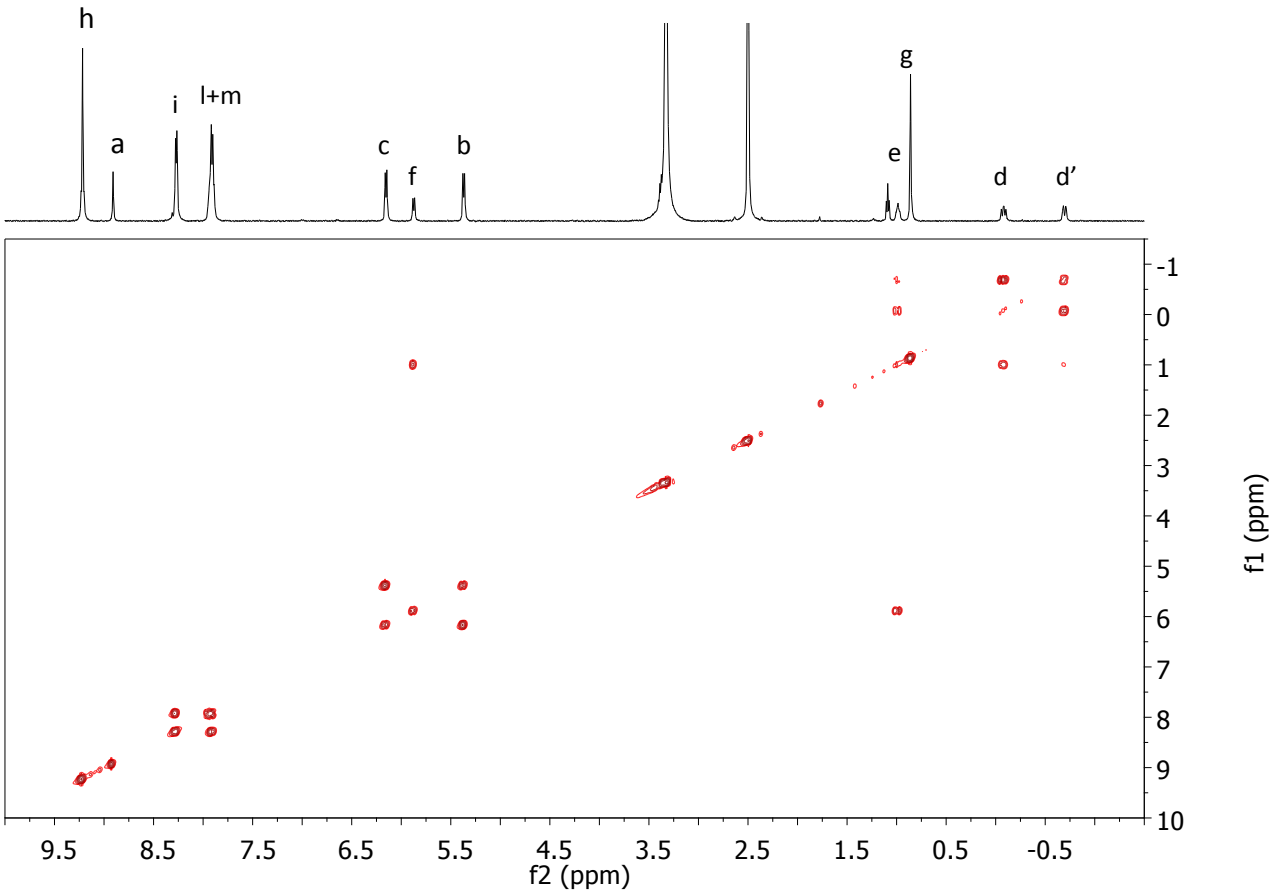

Figure S2. H–H COSY spectrum (dmso-d_6) of **1**.

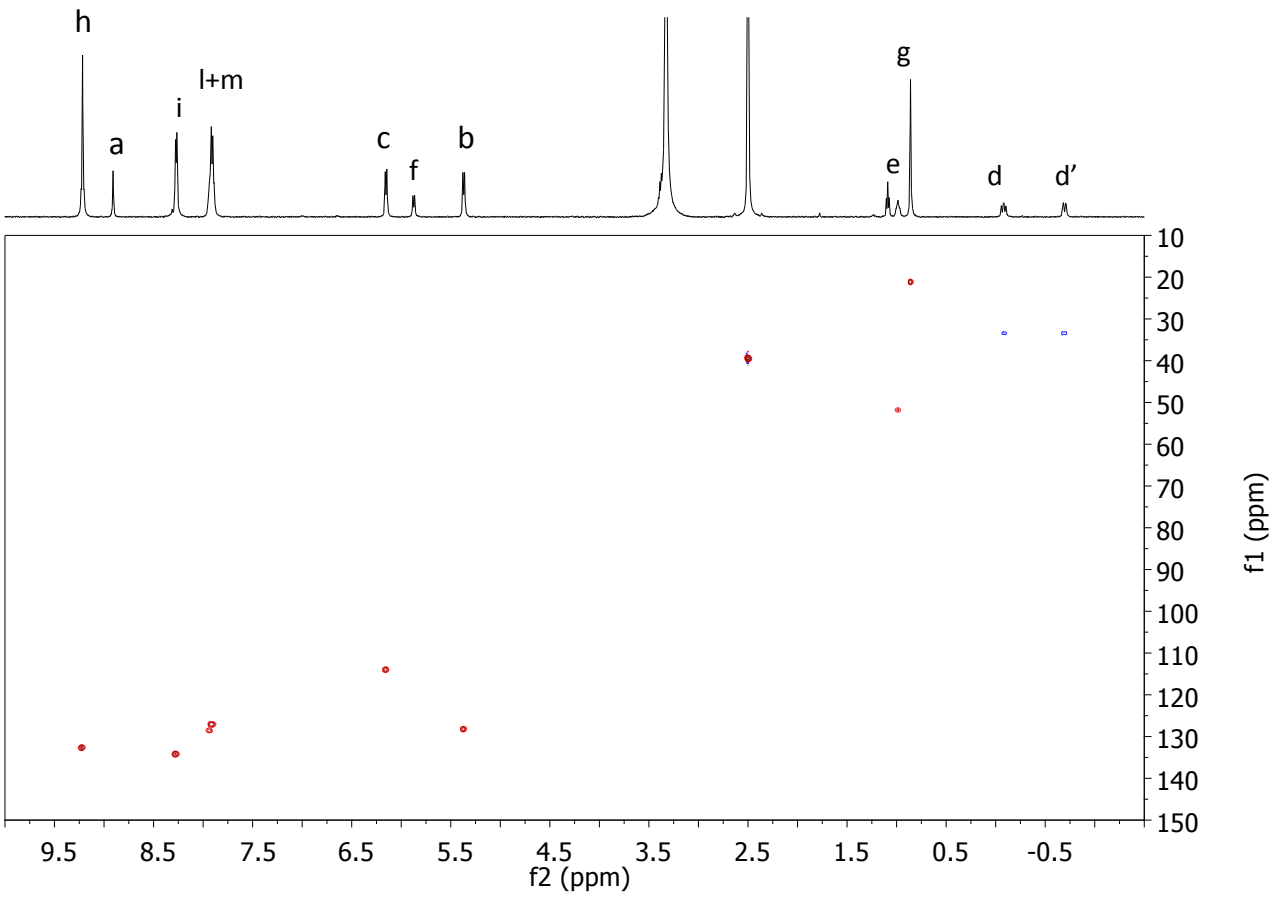

Figure S3. H–C COSY spectrum (dmso-d_6) of **1**.

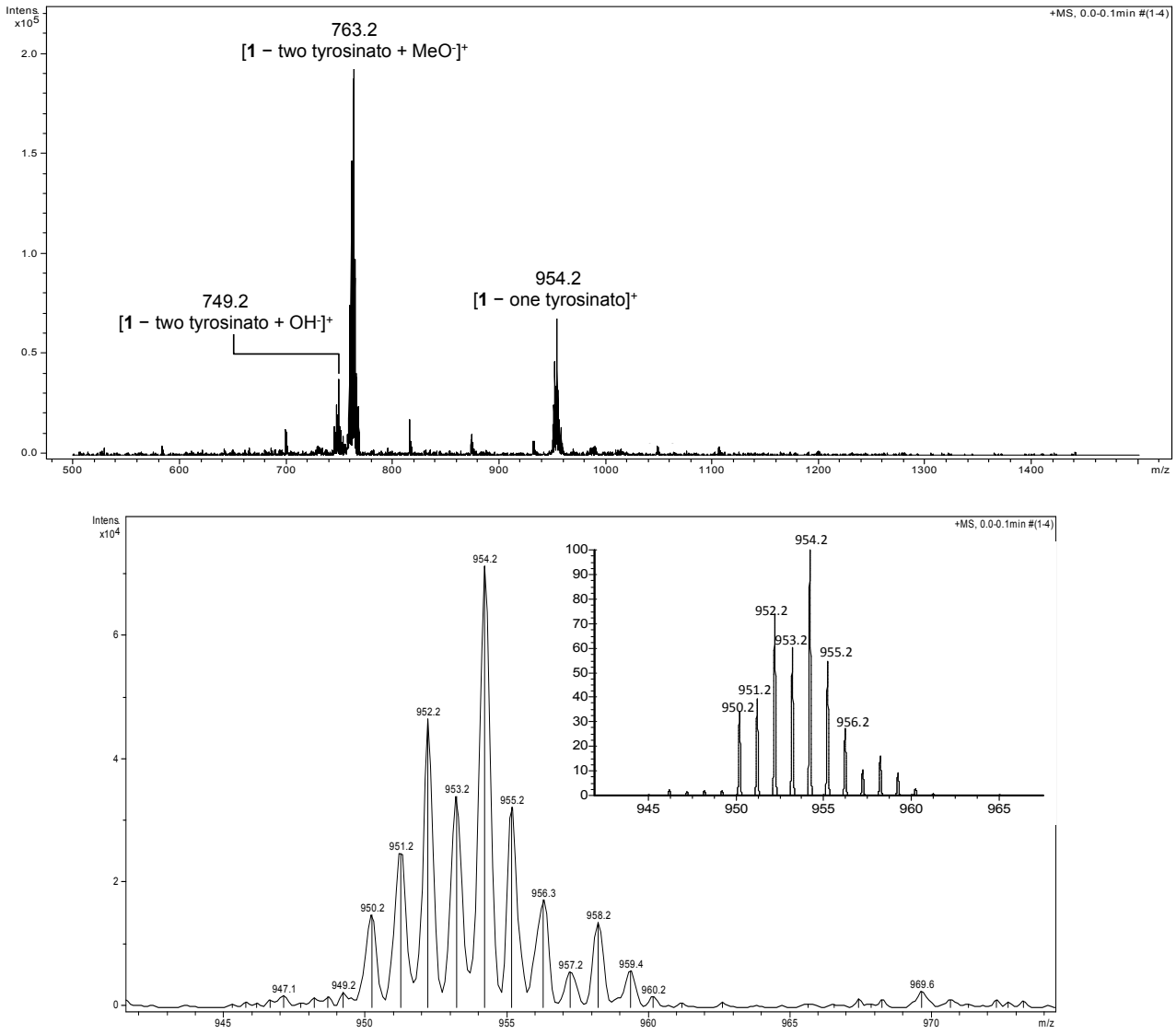

Figure S4. Top: ESI-MS (*m/z*) (positive mode) of **1**. Bottom: experimental and calculated (program IsoPro3, inset) isotopic distributions of the [**1** − one tyrosinato]$^+$ peak centered at *m/z* 954.2.

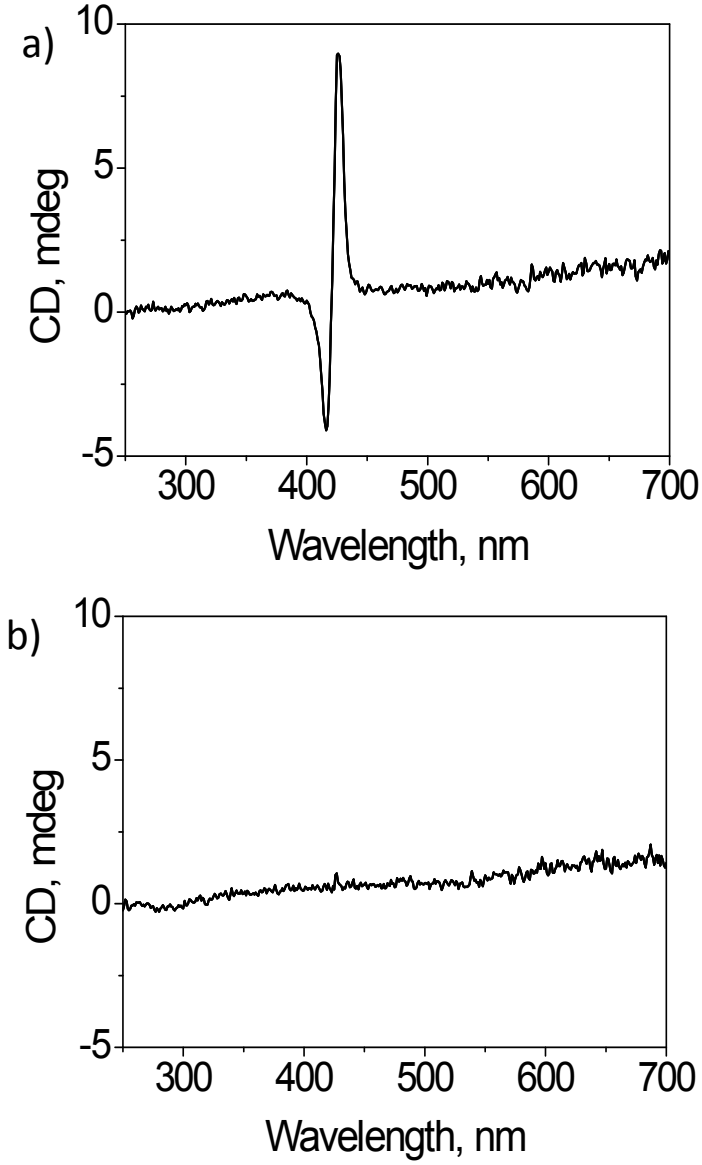

Figure S5. Circular dichroism (CD) spectra of 25 μM dichloromethane solutions of **1** (a) and **2** (b).

S3. Crystallographic data for 1

CCDC 1813181 contains the supplementary crystallographic data for compound **1**. These data can be obtained free of charge from The Cambridge Crystallographic Data Centre *via* https://www.ccdc.cam.ac.uk/structures. SnP-TyrOH crystallizes in the chiral P_1 space group with one entire complex found in the crystallographic asymmetric unit (Figure 1 of the main article and Figure S6). The tin coordination sphere presents bond lengths and angles in line to those reported for similar conjugates;[S12,S13] the two tyrosyl residues, related by a pseudo binary axis, present the expected C_α stereocenter (*S*) configurations (see Table S1 and S2 for detailed crystallographic data). The two planes containing the phenol rings are found to be almost orthogonal to the mean plane containing the porphyrin macrocycle (Figure S6, bottom). In the triclinic crystal form of **1**, CH···π interactions between peripheral phenyl rings of neighbouring porphyrins are found. Hydrogen bonds between the hydroxyl and carbonyl groups of equivalent tyrosyl residues of adjacent unit cells ($d_{OH\cdots OC}$ = 2.679(7) Å and $d_{OH\cdots OC}$ = 2.650(6) Å, Figure S7), develop arrays of **1** along the *a* crystallographic axis. Networks of well-ordered acetone molecules result from hydrogen interactions between the NH amino acid terminals and the solvent carbonyl groups ($d_{NH\cdots OC}$ = 3.39(1) Å and $d_{NH\cdots OC}$ = 3.02(1) Å, Figure S8).

Table S1. Crystallographic data and refinement details for **1**.

	1·2$(CH_3)_2CO$·2$(C_2H_5)_2O$ [$C_{66}H_{46}N_6O_8Sn$·2C_3H_6O·2$C_4H_{10}O$]
CCDC Number	1813181
Chemical Formula	$C_{80}H_{84}N_6O_{12}Sn$
Formula weight (g/mol)	1440.22
Temperature (K)	100(2)
Wavelength (Å)	0.700
Crystal system	Triclinic
Space Group	*P* 1
Unit cell dimensions	*a* = 9.756(2) Å
	b = 13.413(3) Å
	c = 14.922(3) Å
	α = 112.87(3)°
	β = 100.33(3)°
	γ = 94.47(3)°
Volume (Å^3)	1746.5(7)
Z	1
Density (calculated) (g·cm^{-3})	1.369
Absorption coefficient (mm^{-1})	0.412
F(000)	752
Crystal size (mm^3)	0.03 x 0.03 x 0.01
Crystal habit	Pale yellow thick rods
Theta range for data collection	1.50° to 30.97°
Resolution (Å)	0.68
Index ranges	-13 ≤ h ≤ 13
	-19 ≤ k ≤ 19
	-21 ≤ l ≤ 21
Reflections collected	37846
Independent reflections (data with I>2σ(I))	19922 (19635)
Data multiplicity (max resltn)	3.26 (2.61)
I/σ(I) (max resltn)	34.10 (22.71)
R_{merge} (max resltn)	0.0391 (0.0530)
Data completeness (max resltn)	94.5% (86.9%)
Refinement method	Full-matrix least-squares on F^2
Data / restraints / parameters	19922 / 12 / 738
Goodness-of-fit on F^2	1.057
Δ/σ_{max}	0.018
Final R indices [I>2σ(I)][a]	R_1 = 0.0400, wR_2 = 0.1060
R indices (all data)[a]	R_1 = 0.0406, wR_2 = 0.1066
Flack x parameter	0.025(4)
Largest diff. peak and hole (e·Å^{-3})	0.704 and -1.376
R.M.S. deviation from mean (e·Å^{-3})	0.097

[a] $R_1 = \Sigma \; ||Fo|-|Fc|| \; / \; \Sigma \; |Fo|$, $wR_2 = \{\Sigma \; [w(Fo^2 - Fc^2)^2] \; / \; \Sigma \; [w(Fo^2)^2]\}^{½}$

Table S2. Selected bond distances and angles for **1**.

1

Distances	(Å)	**Angles**	**(°)**
Sn_1-NBD_2	2.0750(46)	NBD_2-Sn_1-NAW_2	90.01(18)
Sn_1-NAW_2	2.0818(45)	NBD_2-Sn_1-OXT_3	97.21(16)
Sn_1-NAP_2	2.0937(43)	NBD_2-Sn_1-NAP_2	178.88(25)
Sn_1-NAF_2	2.1056(48)	NBD_2-Sn_1-OXT_5	93.19(16)
Sn_1-OXT_3	2.0887(34)	NBD_2-Sn_1-NAF_2	89.61(18)
Sn_1-OXT_5	2.1019(32)	NAW_2-Sn_1-OXT_3	89.99(16)
		NAW_2-Sn_1-NAP_2	90.27(17)
		NAW_2-Sn_1-OXT_5	93.18(15)
		NAW_2-Sn_1-NAF_2	179.36(25)
		OXT_3-Sn_1-NAP_2	83.87(16)
		OXT_3-Sn_1-OXT_5	169.13(10)
		OXT_3-Sn_1-NAF_2	90.56(16)
		NAP_2-Sn_1-OXT_5	85.72(15)
		NAP_2-Sn_1-NAF_2	90.10(17)
		OXT_5-Sn_1-NAF_2	86.33(16)

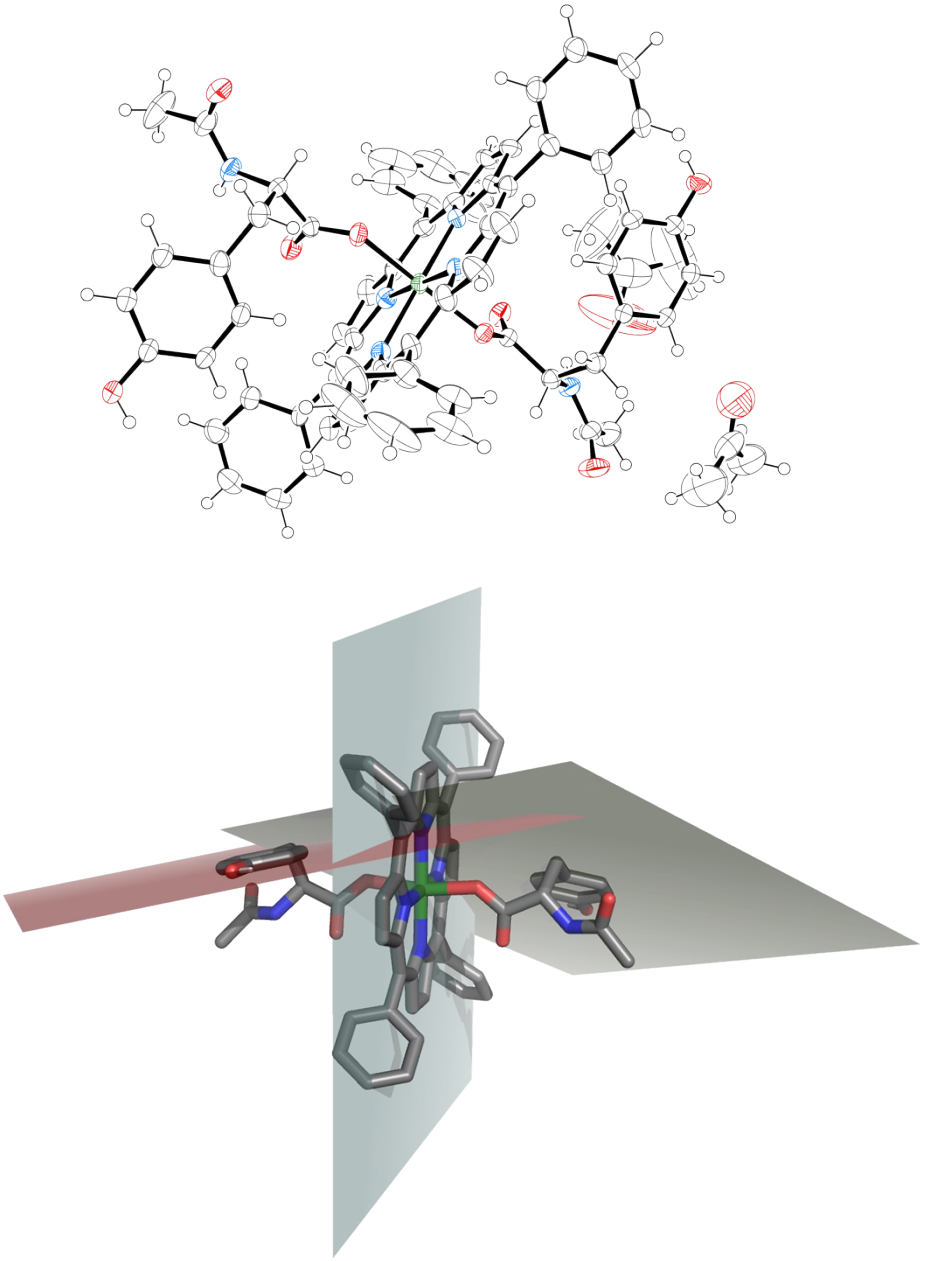

Figure S6. Ellipsoids representation of the crystallographic asymmetric unit content (50% probability) for **1** (top). Detailed view of the X-ray structure of **1** highlighting the mean planes containing the porphyrin macrocycle, light gray, and the two non-equivalent phenol rings, dark gray and red (bottom). The two planes containing the phenols are found to be almost orthogonal to the one containing the porphyrin (average value is 82° - 75.99(6)° between the red and the light gray planes and 88.68(7)° between the dark gray and the light gray ones). The mutual angle between tyrosine sidechains mean planes is 28.94(8)°. Color code: H, white; C, gray; N, blue; O, red; Sn, green.

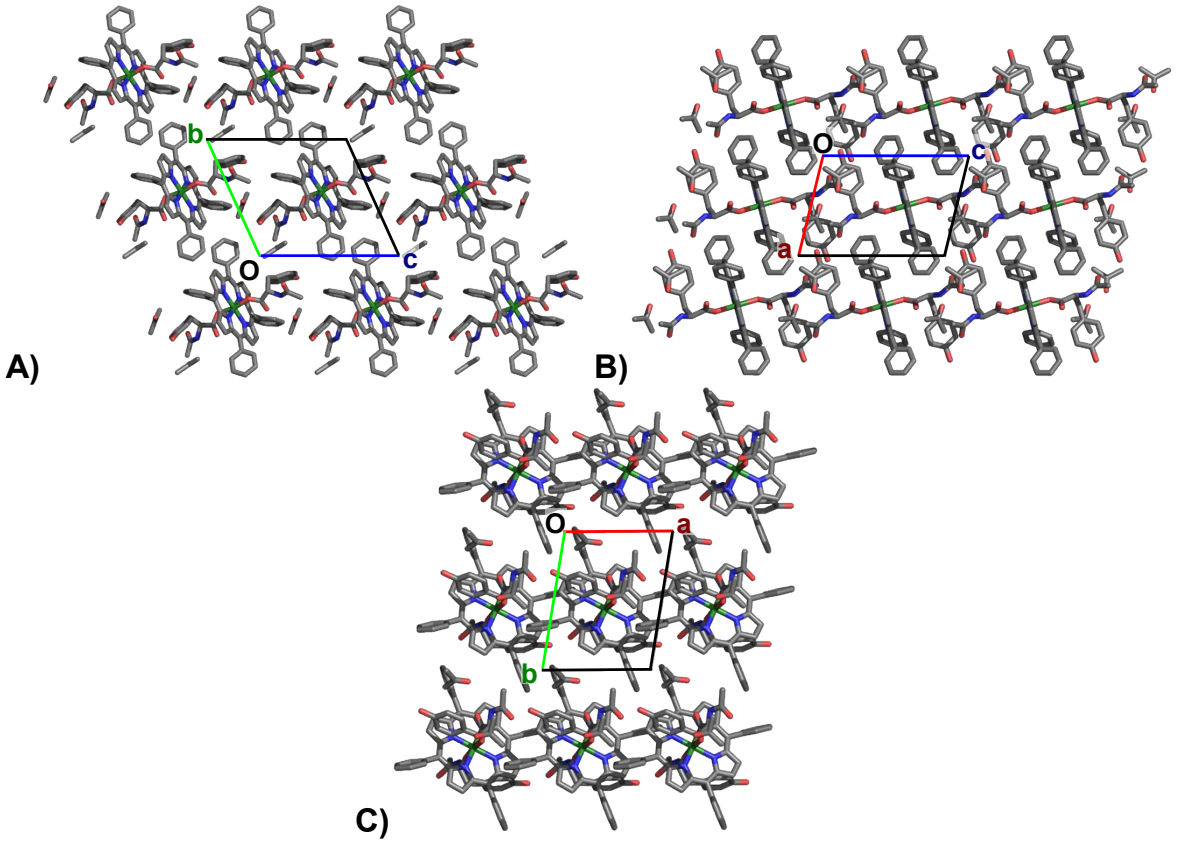

Figure S7. Crystal packing of **1** viewed along the *a*, *b* and *c* crystallographic axes (A, B and C, respectively), hydrogens omitted for clarity. Color code: H, white; C, gray; N, blue; O, red; Sn, green.

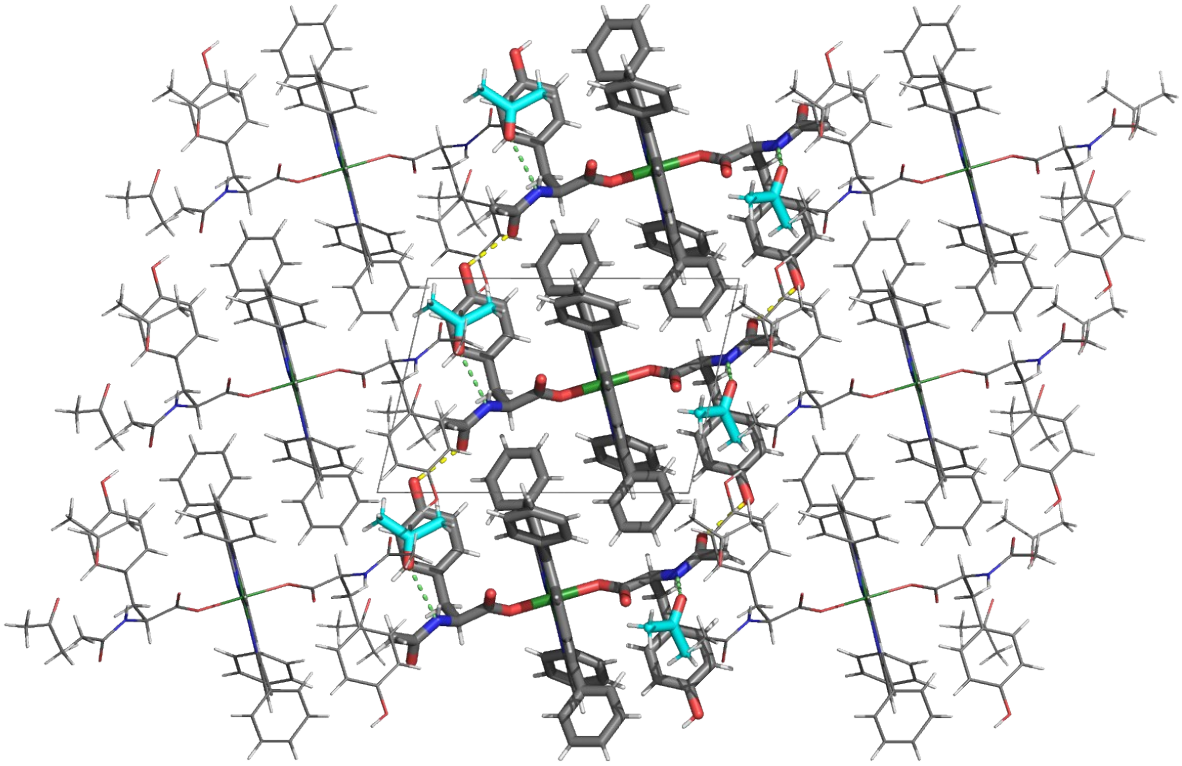

Figure S8. Crystal packing of **1**, viewed along the *b* crystallographic axes, showing the intermolecular H-bonding interactions between phenolic and carbonyl groups of the amino acid residues (yellow dotted lines) and between the NH amidic amino acid terminals and the carbonyl groups of the ordered acetone molecules (green dotted lines). Color code: H, white; C, gray; N, blue; O, red; Sn, green; acetone carbon skeleton, light blue.

S4. Photophysics of 1 and 2 in dichloromethane

S4.1 Absorption spectra

The absorption spectra of **1** and **2** in dichloromethane are reported in Figure S9 and show the typical features (Soret- and Q-bands) of metalloporphyrins of the regular type.[S14] The absorption spectrum of N-acetyl-L-tyrosine is reported in Figure S10 and is dominated by the n-π* electronic transition involving the phenol moiety (maximum at 277 nm).

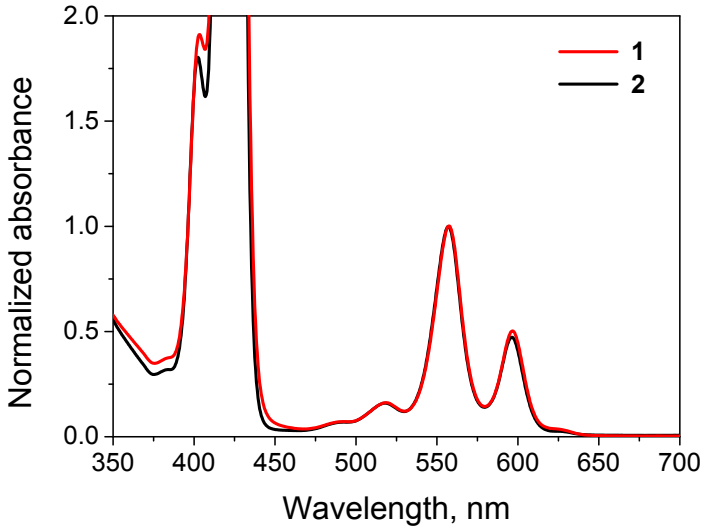

Figure S9. Normalized absorption spectra of **1** and **2** in dichloromethane solution.

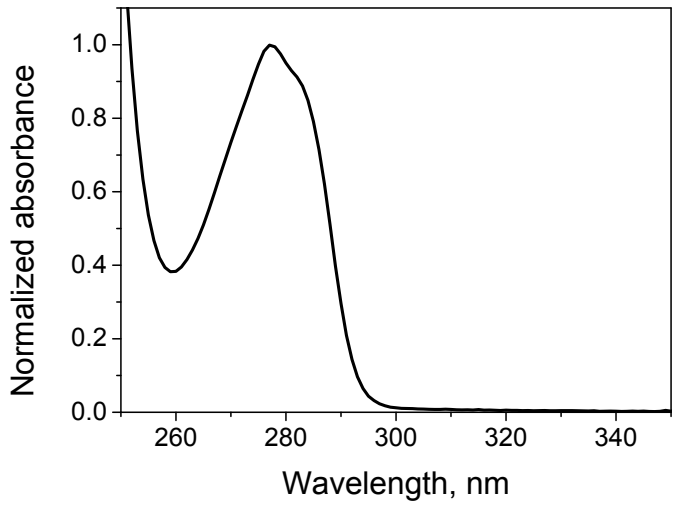

Figure S10. Normalized absorption spectrum of N-acetyl-L-tyrosine in dichloromethane solution obtained by dilution of a concentrated DMF solution (for solubility reasons).

S4.2 Emission spectra

Fluorescence spectra (excitation at 520 nm, optically matched solutions at the excitation wavelength) of **1** and **2** in dichloromethane are reported in Figure S11, showing negligible quenching of the emission in dyad **1**. The lifetime of the porphyrin singlet excited state is comparable for the conjugate **1** and the model system **2** (Figure S12).

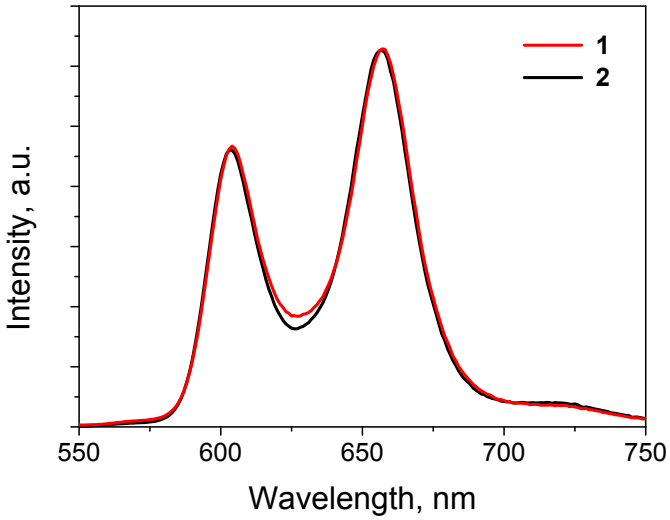

Figure S11. Emission spectra (excitation at 520 nm, optically matched solutions at the excitation wavelength) of **1** and **2** in dichloromethane solution.

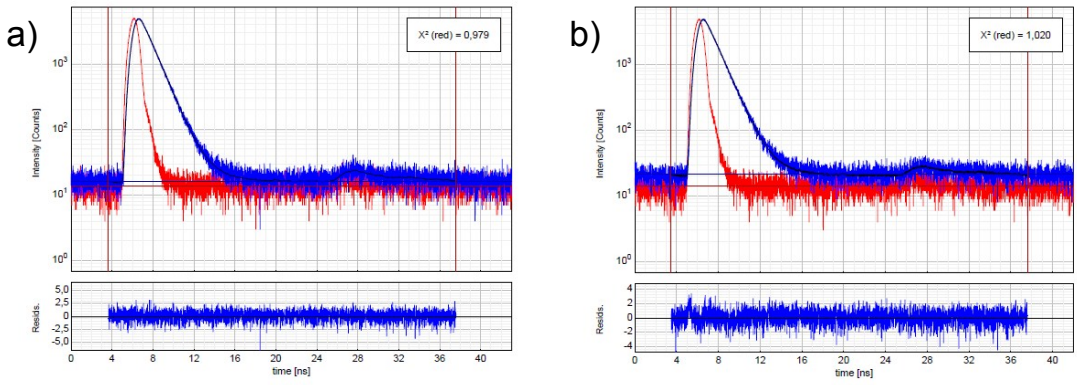

Figure S12. Time-resolved emission decay (excitation at 600 nm, analysis at 660 nm) of a) **1** (lifetime τ = 1.14 ns from the deconvolution and fitting) and b) **2** (lifetime τ = 1.15 ns from the deconvolution and fitting) in dichloromethane solution measured by TC-SPC.

S4.3 Laser flash photolysis

The fraction of SnP singlet excited state that undergoes intersystem crossing to the triplet excited state can be detected by laser flash photolysis. The amount of triplet excited state formed, as well as the corresponding lifetime under both air-equilibrated and oxygen-free conditions, is comparable for **1** and **2** (Figure S13), suggesting negligible quenching in **1** at the triplet level too.

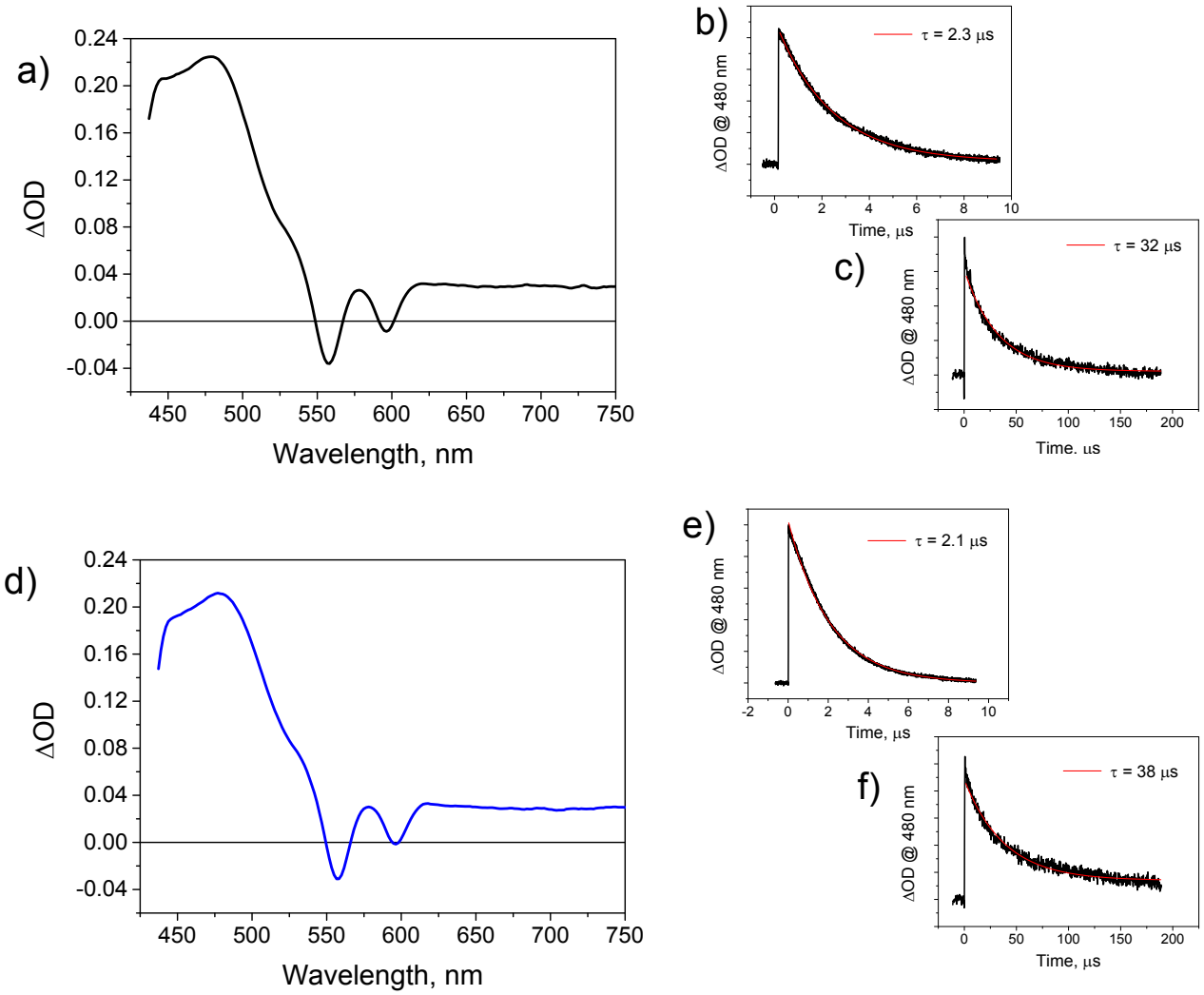

Figure S13. Transient absorption spectra and decays obtained by laser flash photolysis (excitation at 532 nm, optically matched solutions at the excitation wavelength): a) transient spectrum and kinetics of **1** b) in air-equilibrated and c) oxygen-free dichloromethane; d) transient spectrum and kinetics of **2** e) in air-equilibrated and f) oxygen-free dichloromethane.

S5. Electrochemistry

S5.1 Electrochemistry of model compounds 2 and N-acetyl-L-tyrosine

Cyclic voltammetry (CV) experiments have been performed in nitrogen-purged dichloromethane solutions (0.1 M $TBAPF_6$) containing model compounds **2** and N-acetyl-L-tyrosine (1 mM). Addition of the latter has been performed from a 0.1 M solution in DMF (1% dilution). Potentials are referenced vs. Fc/Fc^+ added as internal standard and are reported in Table 1.

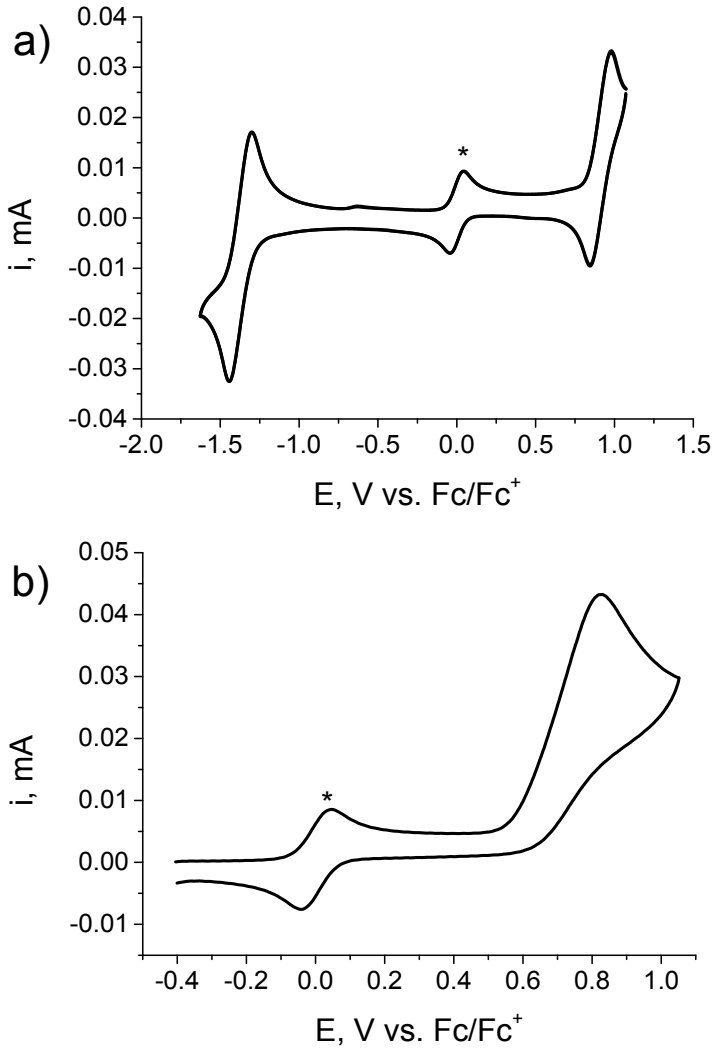

Figure S14. Cyclic voltammetry (CV) of a) **2** and b) N-acetyl-L-tyrosine (with 1% DMF) in nitrogen-purged dichloromethane (0.1 M $TBAPF_6$) at room temperature, scan rate v = 100 mV/s, GC as WE, Pt as CE, SCE as reference, potential referred to the Fc/Fc^+ couple (*).

S5.2 Electrochemistry of 1

Cyclic voltammetry (CV) has been performed in nitrogen-purged dichloromethane solutions (0.1 M $TBAPF_6$) containing **1** (1 mM). 5% DMF was added in order to improve solubility of the conjugate at the concentration required for the electrochemical experiments (solubility in pure dichloromethane solution is restricted to values ≤ 50 μM). Potentials are referenced vs. Fc/Fc^+ added as internal standard and are reported in Table 1.

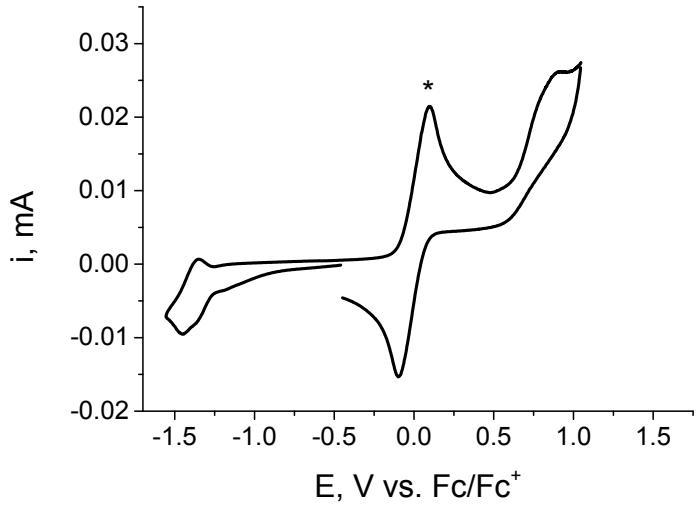

Figure S15. Cyclic voltammetry (CV) of **1** (5% DMF) in nitrogen-purged dichloromethane (0.1 M $TBAPF_6$) at room temperature, scan rate ν = 100 mV/s, GC as WE, Pt as CE, SCE as reference, potential referred to the Fc/Fc^+ couple (*).

S6. Photophysics of 1 in dichloromethane in the presence of pyrrolidine

S6.1 PCET at the singlet level

The attribution of the observed fluorescence quenching to the occurrence of a photoinduced PCET at the singlet level can be supported by the following experimental data:

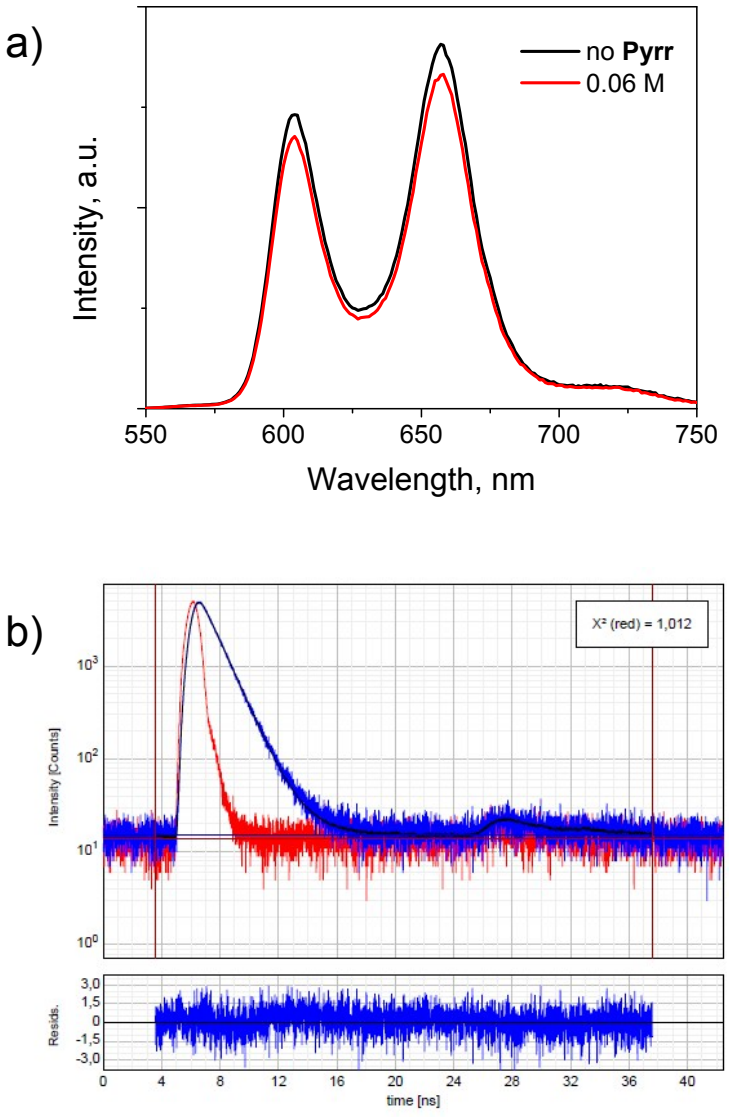

Figure S16. a) Emission spectra (excitation at 520 nm) of **2** in dichloromethane in the absence/presence of 0.06 M pyrrolidine; b) time-resolved emission decay (excitation at 600 nm, analysis at 660 nm) of **2** in dichloromethane solution in the presence of 0.06 M pyrrolidine as measured by TC-SPC (a lifetime of τ = 1.18 ns is estimated from the fitting procedure).

1) Addition of pyrrolidine to a dichloromethane solution of model compound **2** has negligible effects on the SnP singlet excited state emission as it can be observed from the comparison of the fluorescence spectra (excitation at 520 nm) and lifetimes of **2** in the absence/presence of pyrrolidine (Figure S16).

2) Comparison of the absorption spectra (Figure S17) of N-acetyl-L-tyrosine (TyrOH) in the presence/absence of 0.06 M pyrrolidine (Pyr) and that obtained upon addition of excess tetrabutylammonium hydroxide (TBAOH), corresponding to the amino acid with deprotonated phenol group ($TyrO^-$), unambiguously confirms that Pyr does not deprotonate the phenolic moiety of the tyrosine amino acid in dichloromethane (Pyr might deprotonate the carboxylic acid group in the model tyrosine but this process has no relevance in the present investigation). Interestingly, the red-shift observed in the presence of pyrrolidine (maximum at 281 nm) very likely reflects the hydrogen-bonding interaction between the amino acid and the base (see below).

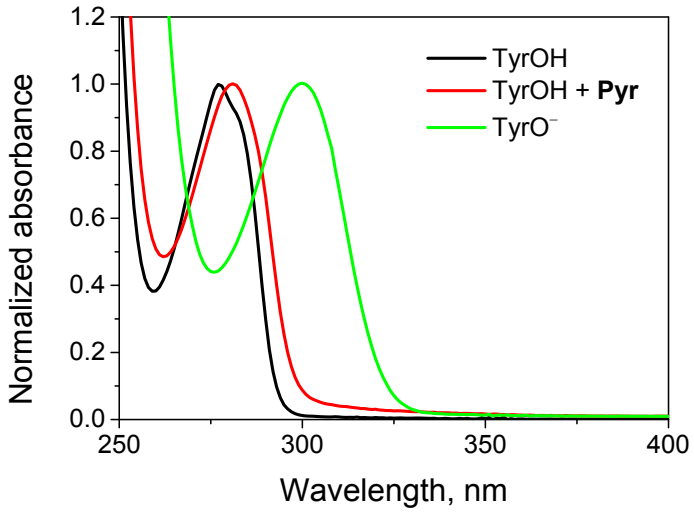

Figure S17. Absorption spectra of 0.5 mM N-acetyl-L-tyrosine in dichloromethane with 1% DMF for solubility reasons (black trace), upon addition of 0.06 M pyrrolidine (red trace), and upon addition of few drops of TBAOH solution (50% in methanol, green trace).

3) The prompt transient spectrum detected by laser flash photolysis of **1** in dichloromethane solution in the presence of 0.06 M pyrrolidine displays larger ΔOD values than the amount of triplet excited state expected on the basis of the singlet excited state quenching (Figure S18a). Since at 0.06 M pyrrolidine the quenching of the singlet in **1** is ca. 60%, according to Figure 2 of the main text, the amount of triplet transient signal should correspond to ca. 40% of the triplet signal in **1** in the absence of pyrrolidine. These observations thus suggest that the prompt transient spectrum is actually composed of the triplet excited state spectrum plus some additional contributions, very likely arising from a PCET state of the type SnP^{-}-$TyrO^{\bullet}$ --- $^{+}HPyr$ which, in the spectral window examined, must display spectral signatures of the SnP radical anion only (the tyrosyl radical indeed has an absorption at 410 nm[S15] of weak intensities which is, in the present case, masked by the strong Soret-band ground-state absorption and therefore not detectable). This consideration can be indeed substantiated by the fact that the prompt transient spectrum of **1** in dichloromethane with added base displays a featuring shoulder at ca 450 nm, which is absent in the differential absorption spectrum of the triplet excited state and is, on the other hand, attributable to the SnP radical anion (Figure S18b). However, simulation of the prompt transient spectrum of Figure S18a (red trace) using a combination of 40% triplet excited state spectrum and 60% of SnP radical anion fails to exactly reproduce the experimental data (Figure S19) and points towards an actual, smaller contribution from the radical pair state in the prompt spectrum. This evidence can be rationalized assuming a partial decay of the PCET state formed via singlet quenching within the time-resolution of the laser flash photolysis experiment (see Section S6.3 for further details).

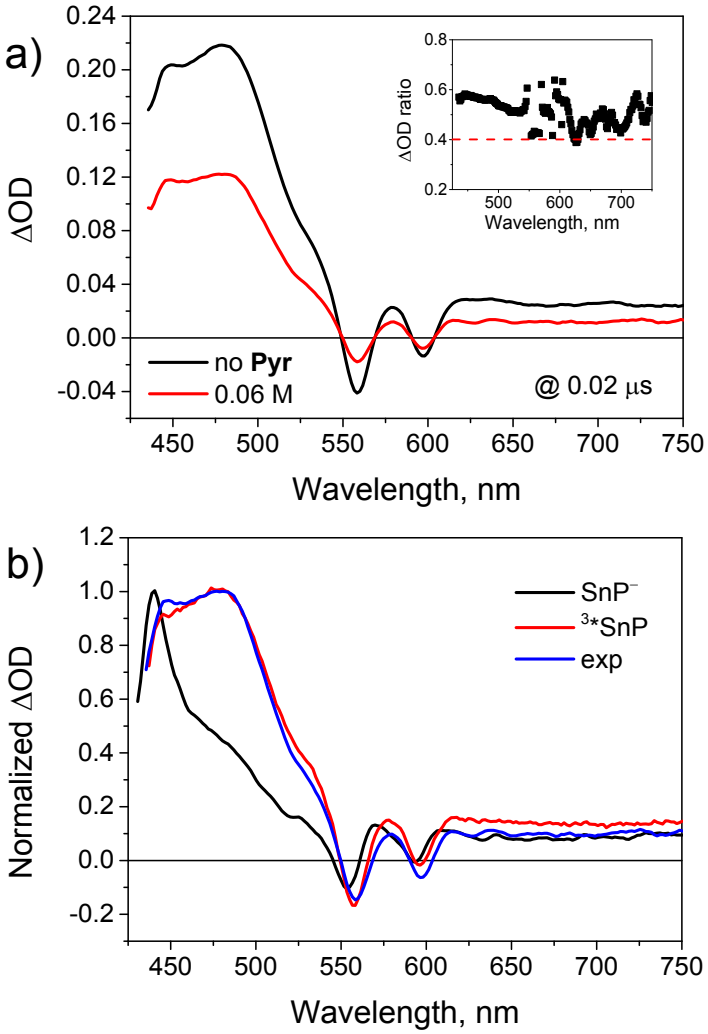

Figure S18. a) Comparison between the prompt transient spectra (0.02 μs time delay) obtained by laser flash photolysis (excitation at 532 nm) of **1** in dichloromethane in the absence (black trace) and presence of 0.06 M pyrrolidine (red trace), the ratio between the two spectra is depicted in the inset; b) comparison of the normalized differential spectra of the SnP radical anion (obtained by laser flash photolysis of **2** in a 95/5 tetrahydrofuran/water mixture in the presence of 10 mM ascorbic acid), of the SnP triplet excited state (obtained by flash photolysis of **2**, Figure S13), and the prompt spectrum (0.02 μs time-delay) obtained by flash photolysis of **1** in dichloromethane with 0.06 M pyrrolidine.

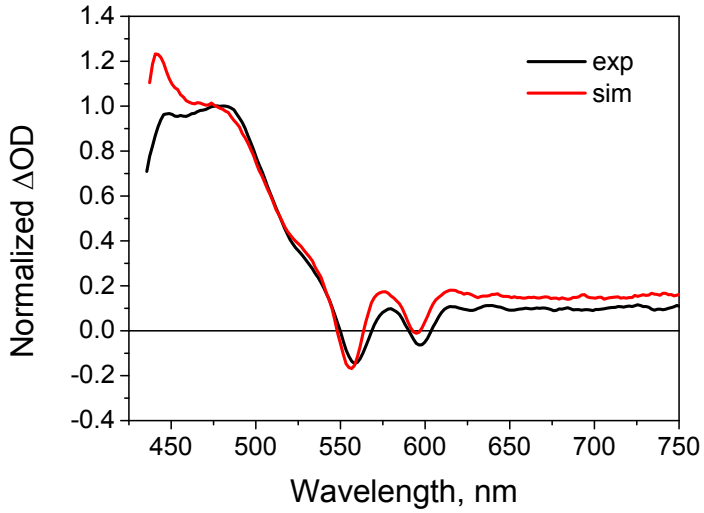

Figure S19. Comparison between the prompt transient spectrum (0.02 μs time delay) obtained by laser flash photolysis (excitation at 532 nm) of **1** in dichloromethane (black trace) in the presence of 0.06 M pyrrolidine and the simulated spectrum using a combination of 40% triplet excited state spectrum and 60% of SnP radical anion (the molar extinction coefficient of the SnP triplet excited state has been determined experimentally using $Ru(bpy)_3^{2+}$ as actinometer, $\Delta\varepsilon$ = 22,000 $M^{-1}cm^{-1}$ at 480 nm; molar extinctions of the transient spectrum of the SnP anion have been taken from the literature).[S16]

S6.2 PCET at the triplet level

Beside the spectral evolution of Figure 4, the attribution of the triplet quenching to the occurrence of a photoinduced PCET at the triplet level can be further confirmed on the basis of the following blank experiment involving model compound **2** and pyrrolidine. As a matter of fact, addition of pyrrolidine to a solution of **2** leads only to a minor quenching (Figure S20a) likely attributable to bimolecular reductive electron transfer since amines can be involved in oxidation reactions being typically used as sacrificial donors, e.g., in photochemical hydrogen evolution experiments.[S17] In spite of the poor efficiency of this quenching process, a bimolecular rate constant can be estimated using a classical Stern-Volmer treatment (Figure S20b) from which a rate constant of $k_Q = 7.5 \cdot 10^5$ $M^{-1}s^{-1}$ can be

extracted. It should be pointed out, however, that this is an approximate value since the high pyrrolidine concentrations used may actually cause specific ground-state interactions between the porphyrin and its environment thus leading to not perfect bimolecular conditions in which the Stern-Volmer treatment should actually be applied (the not perfect linearity of this correlation seems to be consistent with this notion).

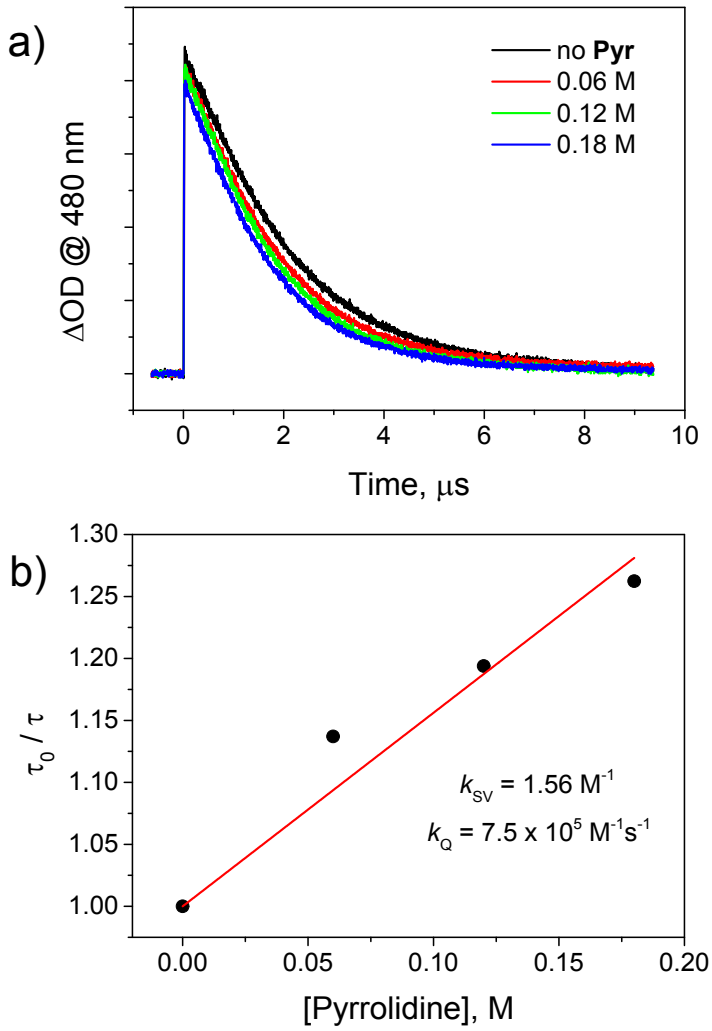

Figure S20. a) Transient absorption decay of the triplet excited state of SnP measured at 480 nm obtained by laser flash photolysis (excitation at 532 nm) of air-equilibrated dichloromethane solutions containing **2** and 0-0.18 M pyrrolidine; b) Stern-Volmer treatment of the quenching process to obtain the bimolecular rate constant (k_Q).

S6.3 Quantum yield of radical pair state formation

The spectral evolution of Figure 4 (main text) shows the formation of the PCET state within a μs which is compatible with the spectrum of the SnP radical anion only. The quantum yield of formation of the long-lived radical pair state can be estimated according to the following calculation (eq S1) where ΔOD, Δε, and Φ are the differential absorbance, the molar extinction coefficient, and quantum yield, respectively, for the reference (R) and the sample (S). Herein we chose $Ru(bpy)_3^{2+}$ in water as reference (actinometer) having $\Delta\varepsilon^R = -10{,}600\ M^{-1}cm^{-1}$ and $\Phi^R = 1$ for the triplet excited state.[S18]

$$\Phi^S = \frac{\Delta OD^S \cdot \Delta\varepsilon^R \cdot \Phi^R}{\Delta OD^R \cdot \Delta\varepsilon^S} \qquad \text{(S1)}$$

We first considered the transient absorption spectrum at 0.9 μs time-delay from Figure 4 as the fingerprint of the SnP^{-}-$TyrO^{\bullet}\cdots{}^{+}HPyr$ state (i.e., SnP radical anion), at this time most of the triplet has already decayed and the radical pair state completely formed. In these conditions the absorption signal at 450 nm can be thus reasonably attributed to the SnP radical anion only. The value obtained is $\Delta OD^S = 0.047$. We then performed a flash photolysis experiment on a $Ru(bpy)_3^{2+}$ aqueous solution optically matched at the excitation wavelength (532 nm) and measured a differential absorbance of $\Delta OD^R = -0.12$ at 450 nm. Using a $\Delta\varepsilon^S = \sim 14{,}000\ M^{-1}cm^{-1}$ at 450 nm for the SnP radical anion (as possibly inferred from a related species of a tin(IV) porphyrin analog),[S16] a quantum yield of $\Phi^S = \sim 0.3$ can be calculated from eq S1. This value is comparable to the value of $\Phi^{S,theor} = 0.32$ as theoretically estimated from the product of the quantum yield of the intersystem crossing to the triplet in dyad **1** ($\Phi_{isc} = 0.365 \cdot 0.9 = 0.33$)[S19] and the triplet quenching yield ($\Phi_q = 0.98$ under oxygen-free conditions, see below Table S4). This result thus points towards the fact that singlet quenching and triplet quenching by PCET bring to radical pair states of different spin multiplicity in which the singlet undergoes rapid decay, whose kinetics is not detected by laser flash photolysis experiment (a hint is observed solely in the prompt spectrum, see Figure S18) and only the triplet PCET state is followed as a long-lived species.

S6.4 Detailed kinetic data

The following tables summarize all the kinetic data of **1** in the presence of pyrrolidine experimentally obtained by spectroscopic techniques and related kinetic treatment.

Table S3. Singlet excited state quenching by photoinduced PCET.

[Pyr], M	τ (ns)[a]	k_{obs} (10^8 s^{-1})	Quenching yield[b]	Quenching yield[c]
0	1.15	8.7	/	/
0.012	0.64	15.6	0.444	0.488
0.024	0.46	21.7	0.600	0.559
0.036	0.45	22.2	0.609	0.592
0.048	0.44	22.7	0.617	0.621
0.060	0.42	23.8	0.635	0.626
0.072	0.42	23.8	0.635	0.635
0.084	0.41	24.3	0.644	0.640

[a]Obtained by TC-SPC excitation at 600 nm, analysis at 660 nm; [b]using lifetime data; [c]using steady-state fluorescence data (Figure 2 of the main text).

Table S4. Triplet excited state quenching by photoinduced PCET.[a]

[Pyr], M	τ_1 (μs)[b]	τ_1 (μs)[c]	τ_2 (μs)[c]	Quenching yield[b]	Quenching yield[c]	k_{obs} (10^5 s^{-1})[c]
0	2.34	32	/	/	/	0.5
0.012	0.84	0.96	6.9	0.641	0.952	10.3
0.024	0.62	0.64	6.9	0.735	0.968	15.6
0.036	0.50	0.47	5.6	0.785	0.976	21.3
0.048	0.44	0.41	6.2	0.812	0.979	24.3
0.060	0.41	0.38	5.5	0.823	0.981	26.3
0.072	0.38	0.37	5.6	0.836	0.982	27.0
0.084	0.37	0.35	6.0	0.844	0.982	28.5

[a]Obtained by laser flash photolysis (excitation at 532 nm) from the transient decay at 480 nm; [b]from the first component of a biexponential fitting of kinetic traces under air-equilibrated conditions (see Figure 3a of the main text); [c]from a biexponential fitting of kinetic traces under oxygen-free conditions (see Figure S24a for selected traces).

S6.5 Energy level diagram

The energy level diagram depicted in Figure 5 of the main text has been constructed according to a combination of photophysical, electrochemical, and protonation data as follows.

a) **SnP-TyrOH···Pyr level**: it corresponds to the ground state and an energy of 0.0 eV has been set.

b) **^{1}*SnP-TyrOH···Pyr level**: it corresponds to the lowest energy singlet excited state (S_1) of the SnP and its value, +2.08 eV, has been estimated from the wavelength at the intersection between normalized absorption and fluorescence spectra.

c) **^{3}*SnP-TyrOH···Pyr level**: it corresponds to the lowest energy triplet excited state (T_1) of the SnP and its value, +1.65 eV, has been taken from literature data.[S19]

d) **SnP$^{–}$-TyrOH$^{•+}$ level** (gray line): it corresponds to the radical pair state in the absence of any base and its value, +2.20 eV, has been calculated from the difference between the oxidation potential of the model N-acetyl-L-tyrosine and the reduction potential of SnP in model compound **2** (Table 1, main text). Importantly, this state is up-hill with respect to both singlet (by 0.12 eV) and triplet (by 0.55 eV) excited states, thus justifying the lack of quenching of both states in the absence of added pyrrolidine base.

e) **SnP$^{–}$-TyrOH$^{•}$···$^{+}$HPyr level**: it corresponds to the PCET state with pyrrolidine as a base and it has been estimated considering the energy of the radical pair state without base (point d) and subtracting the contribution from the deprotonation step. The latter has been taken according to eq S2. For the sake of simplicity, the possible energy difference between the singlet and triplet radical pair states, which is related to the spin-spin exchange integral *J*, has been neglected and the same energy has been thus assumed for both states.

$$\Delta G_{PT} = 0.059 \text{ eV} \cdot [pK_a (TyrOH^{•+}) – pK_a (^{+}HPyr)] \quad (S2)$$

In the absence of suitable values for pK_a ($TyrOH^{•+}$) in organic solvents and, in general, for organic acids in dichloromethane, we decided to consider pK_a values for both acids in acetonitrile. However, in place of the pK_a value corresponding to the protonated tyrosyl radical, the pK_a value for the radical of 2,4,6-tri-*tert*-butylphenol ($PhOH^{•+}$), known from the literature, was used.[S20]

These data are: pK_a ($^+$HPyr) = 19.65;[S21] pK_a ($PhOH^{\bullet+}$) = –3.[S20]

Once put into eq S2, a ΔG_{PT} value of 1.3 eV can be obtained, yielding an energy for the PCET product of +0.9 eV. This value has to be taken with caution since it implies several approximations as specified above (protonation data in acetonitrile, different phenol derivative) and should be considered, with quite confidence, as a lower limiting value according to the following. 2,4,6-tri-*tert*-butylphenol displays a more positive oxidation potential[S20] than N-acetyl-L-tyrosine (E = +1.18 V and E = +0.99 V vs. Fc/Fc^+, respectively), thus, in spite of the different solvent used, it can be reasonably argued that once the phenoxyl radical has been formed the $PhOH^{\bullet+}$ radical is expected to be a stronger acid than the $TyrOH^{\bullet+}$ radical (this trend is somewhat confirmed by literature data).[S20] Accordingly, since it can be considered that pK_a ($TyrOH^{\bullet+}$) ≥ –3, it directly follows that $\Delta G_{PT} \leq 1.3$ eV and thus the energy of the PCET photoproduct is ≥ +0.9 eV.

f) **SnP-TyrOH$^-$···$^+$HPyr level**: it corresponds to the state where the backward reaction has already occurred by only an ET process from SnP radical anion to the tyrosyl radical while the proton is still at the pyrrolidine. It has been estimated considering, similarly to the previous case, the pK_a value of 2,4,6-tri-*tert*-butylphenol and pK_a of pyrrolidinium in acetonitrile,[S20,S21] being 28 and 19.65, respectively. Accordingly, the ΔG_{PT} estimated by eq S2 is +0.5 eV. For similar reasons as above, this value obtained should be considered as a lower limiting one (≥ +0.5 eV).

S6.6 Kinetic treatment and determination of k_{CPET}

When dealing with CPET processes, a double tunneling approximation is usually invoked to account for the kinetics. Since protons cannot tunnel as fast as electrons, a pre-association equilibrium involving hydrogen bonding between the tyrosine and the pyrrolidine base must be considered (eq S3), whose thermodynamics is accounted for by the association constant K_A (eq S4).

$$TyrOH + Pyr \leftrightarrow TyrOH \cdots Pyr \quad \text{(S3)}$$

$$K_A = \frac{[TyrOH \cdots Pyr]}{[TyrOH][Pyr]} \quad \text{(S4)}$$

This thus means that the actual rate for CPET ($k_{CPET,exp}$) is the product of the rate constant (k_{CPET}) multiplied by the fraction of associated species according to eq S5 and is thus dependent on the pyrrolidine concentration.

$$k_{CPET,exp} = k_{CPET} \frac{[TyrOH \cdots Pyr]}{[TyrOH] + [TyrOH \cdots Pyr]} \quad \text{(S5)}$$

By appropriately rearranging eq S5 using eq S4 the following expression can be obtained (eq S6).

$$k_{CPET,exp} = k_{CPET} \frac{K_A[Pyr]}{1 + K_A[Pyr]} \quad \text{(S6)}$$

The observed rate constant for the decay of both singlet and triplet excited states (k_{obs}) can be split into several contributions arising from all the potential pathways available to the related excited state, according to eq S7.[S22,S23]

$$k_{obs} = k_0 + k_{ET} + k_Q[Pyr] + k_{CPET} \frac{K_A[Pyr]}{1 + K_A[Pyr]} \quad \text{(S7)}$$

In order to obtain the rate constant for the CPET it is important to determine the association constant K_A. The first attempt to this estimate has been performed using the fluorescence data (Figure 2 of the main text), according to the treatment given by T. J. Meyer and coworkers,[S24] from the intercept/slope ratio of the 1/ΔI vs. 1/[**Pyr**] plot (Figure S21), where $\Delta I = I_0 - I$ is the difference between the emission intensity in the absence of pyrrolidine (I_0) and the emission intensity (I) in the presence of pyrrolidine (taken from Figure 2a of the main text). The association constant obtained, however, is substantially higher than the K_A values for hydrogen bonding between phenols and pyridines in dichloromethane experimentally determined by Linschitz and coworkers.[S23] Also, fitting of the k_{obs} data for both singlet and triplet excited state decay according to eq S7 using an association constant of K_A = 215 M^{-1} (Figure S21) leads to completely unreliable results.

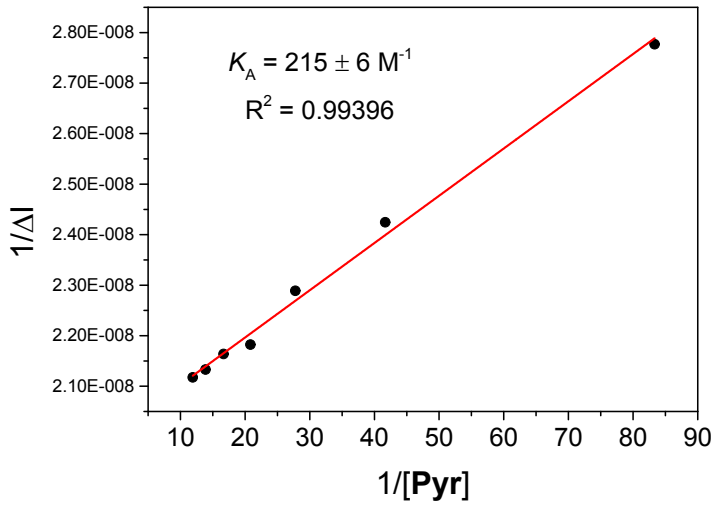

Figure S21. Plot of 1/ΔI vs. 1[**Pyr**] and its linear fitting for the estimation of the association constant K_A according to the treatment by T. J. Meyer and coworkers.[S24]

Therefore, in order to obtain suitable values for both K_A and k_{CPET} we decided to fit the data k_{obs} *vs.* [Pyrrolidine] for both singlet and triplet excited state decay according to eq S7 by forcing a common value for the association constant K_A.[S22] This mathematical treatment leads to more reliable results, with fitting data showing good statistics (Figure S22).

Singlet excited state decay

When considering singlet excited state decay according to eq S7, simple electron transfer (k_{ET}) can be neglected according to the comparable singlet lifetime measured in **1** and **2** (Figure S12), also direct quenching by the base (k_Q[Pyr]) can be safely discarded due to the comparable fluorescence lifetime of model compound **2** in the presence and in the absence of pyrrolidine (Figure S17), thus eq S7 reduces to eq S8, where $k_0 = 8.7 \cdot 10^8$ s^{-1} is obtained from the lifetime of the singlet excited state in **1** in the absence of pyrrolidine.

$$k_{obs} = k_0 + k_{CPET} \frac{K_A[Pyr]}{1 + K_A[Pyr]} \qquad \text{(S8)}$$

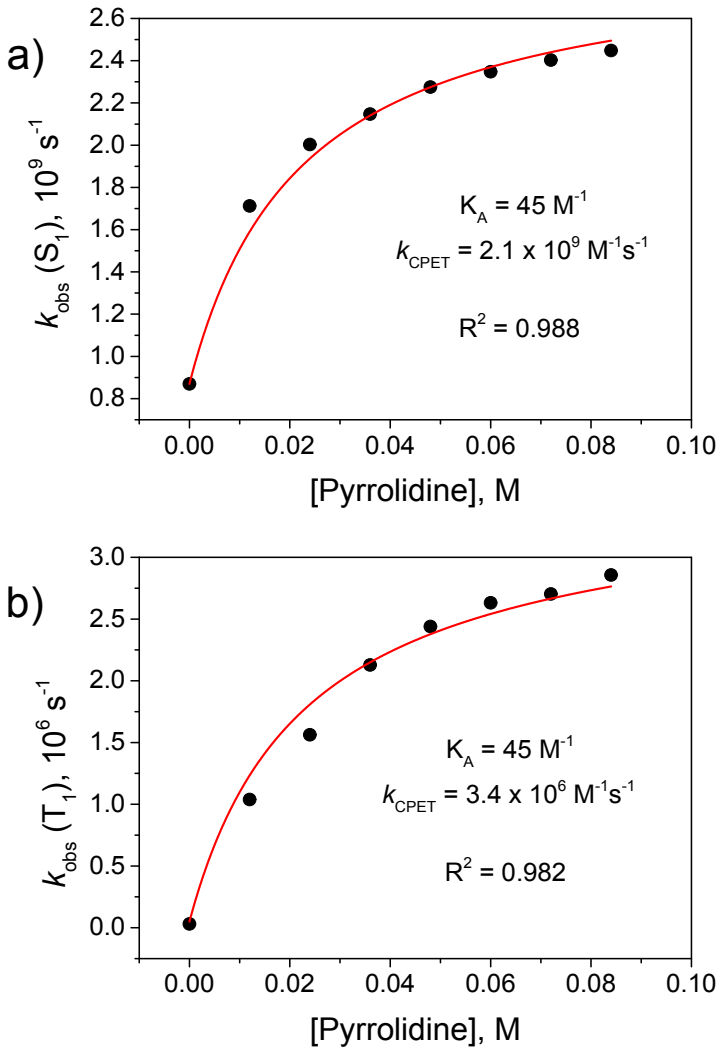

Figure S22. Mathematical treatment of the observed rate for a) singlet and b) triplet excited state decay (oxygen-free conditions) according to eq S7 by forcing a common K_A value.

Triplet excited state decay

When considering triplet excited state decay according to eq S7, simple electron transfer (k_{ET}) can be reasonably neglected due to the comparable triplet lifetime of **1** and **2** (Figure S13), thus eq S7 reduces to eq S9, where $k_0 = 3.1 \cdot 10^4$ s^{-1} is obtained from the lifetime of the triplet excited state in the absence of pyrrolidine under oxygen-free conditions and $k_Q = 7.5 \cdot 10^5$ $M^{-1}s^{-1}$ is obtained from the triplet quenching data of **2** in the presence of pyrrolidine (Stern-Volmer treatment, Figure S20).

$$k_{obs} = k_0 + k_Q[Pyr] + k_{CPET}\frac{K_A[Pyr]}{1 + K_A[Pyr]} \quad \text{(S9)}$$

Fitting of both observed rates by forcing a common K_A value yields the following data:

k_{CPET} (S_1) = 2.1(±0.03)·10^9 s^{-1}; k_{CPET} (T_1) = 3.4(±0.08)·10^6 s^{-1}; K_A = 45(±5) M^{-1}.

The value of K_A obtained from this analysis is comparable with previous association constants reported by Linschitz and coworkers for hydrogen-bonding equilibriums in CH_2Cl_2 between phenols and pyridines.[S23] In order to additionally strengthen the consistence of the approach adopted and of the rate constants for the CPET processes so obtained, we performed an independent evaluation of the association constant K_A by performing a spectrophotometric titration experiment, namely by monitoring the absorption spectrum of the N-acetyl-L-tyrosine model compound in dichloromethane (1% DMF for solubility reasons) in the presence of increasing amount of pyrrolidine.[S25] The data set obtained is reported in Figure S23a: addition of pyrrolidine is indeed followed by an enhancement of the absorption patterns with a concomitant, progressive red-shift, which is consistent with the occurrence of a hydrogen-bonding interaction (eq S3). A non-linear regression treatment of the ΔOD *vs*. [Pyr] (Figure S23), where ΔOD is the difference between the absorbance at a fixed wavelength (A) in the presence of pyrrolidine and the absorbance (A_0) in the absence of the base, according to eq S10,[S25,S26] gives an association constant of K_A = 47(±7) M^{-1}, which is, within experimental error, comparable with the one (K_A = 45(±5) M^{-1}) obtained through the fitting of the kinetic data (see above, Figure S21 and S22).

$$[TyrOH \cdots Pyr] = \frac{[TyrOH]_0 + [Pyr]_0 + K_A{}^{-1}}{2} \mp \sqrt{\left(\frac{[TyrOH]_0 + [Pyr]_0 + K_A{}^{-1}}{2}\right)^2 - [TyrOH]_0[Pyr]_0} \quad \text{(S10)}$$

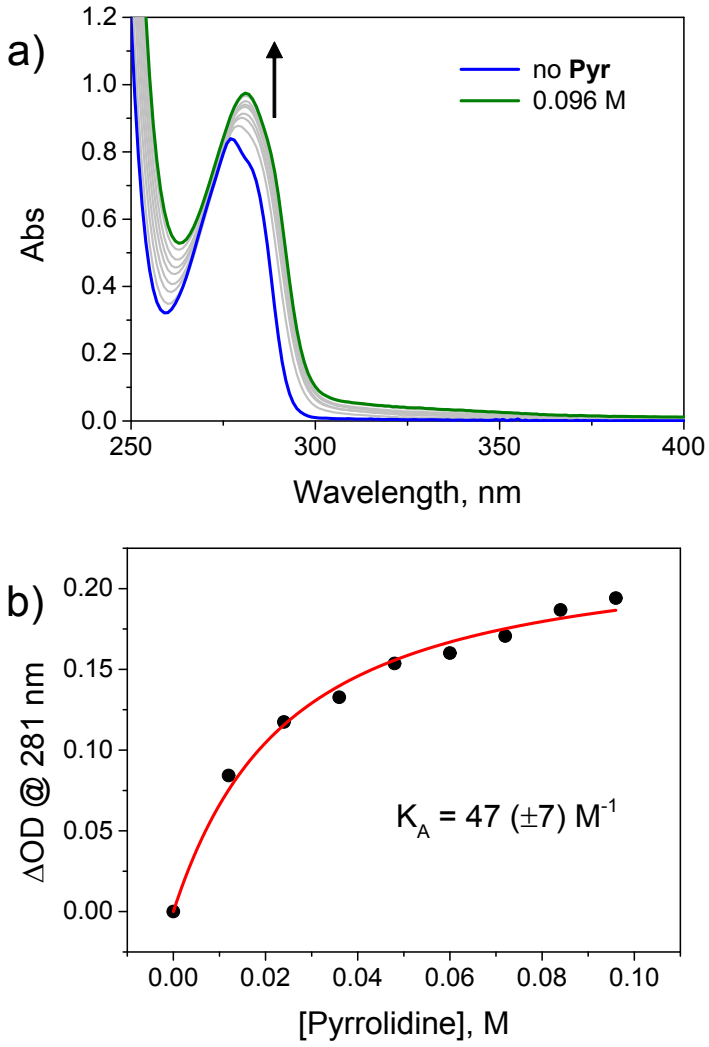

Figure S23. (a) Absorption spectra of 0.5 mM N-acetyl-L-tyrosine in dichloromethane (1% DMF) upon addition of up to 0.096 M pyrrolidine; (b) plot of the difference of absorbance at 281 nm as a function of pyrrolidine concentration and related fitting of the data according to eq S10.

Backward reaction

As discussed in the main text, ground-state repopulation may in principle occur through two different pathways, namely *via* a CPET or a step-wise ET-PT process. Nothing can be said, for the absence of kinetic information, as regarding the PCET state of singlet multiplicity.

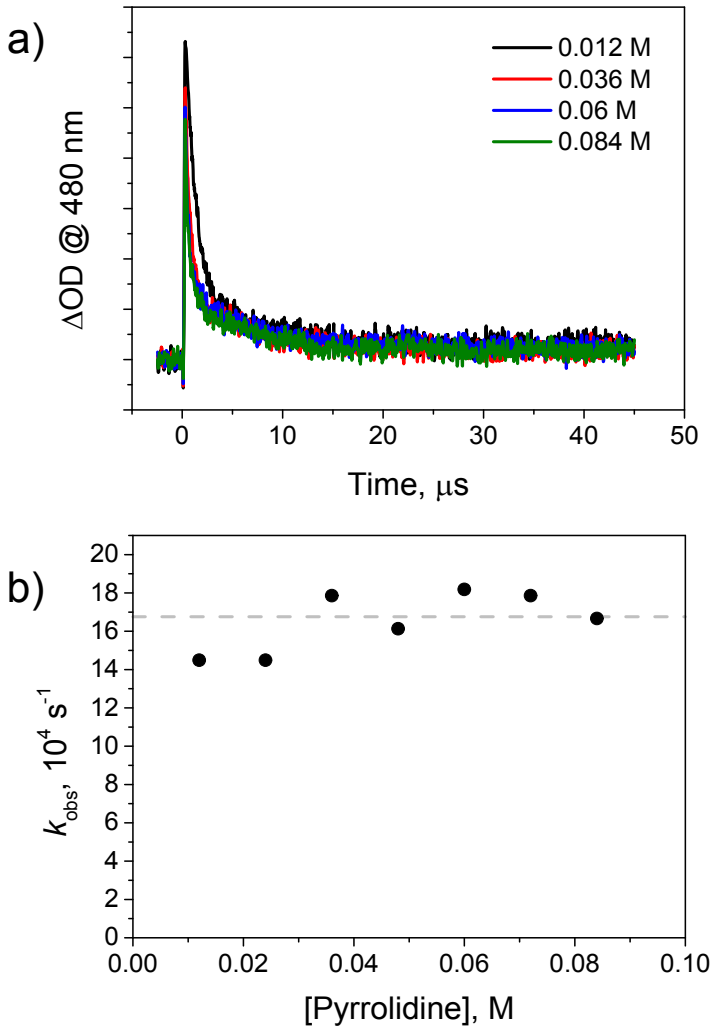

Figure S24. (a) Selected kinetic traces at 480 nm obtained by laser flash photolysis (excitation at 532 nm) of oxygen-free dichloromethane solutions containing **1** and 0-0.084 M pyrrolidine; (b) trend of decaying rates of the PCET state vs. pyrrolidine concentration.

On the other hand, as far as the triplet radical pair state is concerned, although the spectral changes observed cannot unambiguously establish which pathways is actually followed (since the phenolate anion has no fingerprint in the visible spectrum, Figure S17), the observation of appreciably pyrrolidine-independent kinetics (Figure S24, Table S4 for the related data) seems to support the occurrence of an intramolecular reverse electron transfer process leading to the formation of a phenolate intermediate prior to ground-state repopulation.

S6.7 Estimation of the reorganization energy λ of the CPET

The difference in rates between photoinduced CPET at the singlet and triplet levels may be employed to get a rough estimate of the total reorganization energy of the CPET process. Indeed, both rate constants can be described, in a classical Marcus-type treatment, according to eq S11, where *A* is a pre-exponential factors that includes the vibronic coupling between initial and final states, ΔG° is the driving force for the CPET process and λ is the total reorganization energy.

$$k = A \cdot exp\left[-\frac{(\Delta G^0 + \lambda)^2}{4\lambda\, k_B T}\right] \qquad \text{(S11)}$$

If we assume (as reasonably expected) comparable pre-exponential factors for both singlet and triplet PCET states, we can consider the ratio between the rate constants for both processes and, applying the logarithmic function, we can come up with eq S12.

$$2.303(\log k_{CPET}(S_1) - \log k_{CPET}(T_1)) = -\frac{\left[\Delta G^0_{CPET}(S_1) + \lambda\right]^2}{4\lambda\, k_B T} + \frac{\left[\Delta G^0_{CPET}(T_1) + \lambda\right]^2}{4\lambda\, k_B T} \qquad \text{(S12)}$$

Using k_{CPET} (S_1) = $2.1 \cdot 10^9$ s^{-1}, k_{CPET} (T_1) = $3.4 \cdot 10^6$ s^{-1}, $\Delta G°_{CPET}$ (S_1) = 1.1 eV, $\Delta G°_{CPET}$ (T_1) = 0.7 eV as previously estimated (see above), and T = 298 K a total reorganization energy of λ = 1.16 eV can be estimated.

S7. References of the Supporting Information

S1 P. Cavigli, G. Balducci, E. Zangrando, N. Demitri, A. Amati, M. T. Indelli and E. Iengo, *Inorg. Chim. Acta*, 2016, **439**, 61, and references therein.

S2 A. Lausi, M. Polentarutti, S. Onesti, J. R. Plaisier, E. Busetto, G. Bais, L. Barba, A. Cassetta, G. Campi, D. Lamba, A. Pifferi, S. C. Mande, D. D. Sarma, S. M. Sharma and G. Paolucci, *The European Physical Journal Plus* 2015, **130**, 1.

S3 W. Kabsch, *Acta Crystallographica Section D* 2010, **66**, 125.

S4 M. D. Winn, C. C. Ballard, K. D. Cowtan, E. J. Dodson, P. Emsley, P. R. Evans, R. M. Keegan, E. B. Krissinel, A. G. W. Leslie, A. McCoy, S. J. McNicholas, G. N. Murshudov, N. S. Pannu, E. A. Potterton, H. R. Powell, R. J. Read, A. Vagin and K. S. Wilson, *Acta Crystallographica Section D* 2011, **67**, 235.

S5 P. R. Evans and G. N. Murshudov, *Acta Crystallographica Section D* 2013, **69**, 1204.

S6 G. M. Sheldrick, *Acta Crystallographica Section A* 2015, **71**, 3.

S7 P. Emsley, B. Lohkamp, W. G. Scott and K. Cowtan, *Acta Crystallographica Section D* 2010, **66**, 486.

S8 A. Spek, *Acta Crystallographica Section C* 2015, **71**, 9.

S9 S. Parsons, H. D. Flack and T. Wagner, *Acta Crystallographica Section B* 2013, **69**, 249.

S10 L. Farrugia, *Journal of Applied Crystallography* 2012, **45**, 849.

S11 L. Schrodinger, The PyMOL Molecular Graphics System, Schrodinger, LLC, 2015 http://www.pymol.org.

S12 a) T. Honda, T. Nakanishi, K. Ohkubo, T. Kojima and S. Fukuzumi, *J. Phys. Chem. C* 2010, **114**, 14290. b) T. Lazarides, S. Kuhri, G. Charalambidis, M. K. Panda, D. M. Guldi and A. G. Coutsolelos, *Inorg. Chem.* 2012, **51**, 4193. c) P. Cavigli, G. Balducci, E. Zangrando, N. Demitri, A. Amati, M. T. Indelli and E. Iengo, *Inorg. Chim. Acta*, 2016, **439**, 61.

S13 a) S. H. Kim, H. Kim, K. K. Kim and H. J. Kim, *J. Porph. Phthal.* 2009, **13**, 806. b) K. Karikis, E. Georgilis, G. Charalambidis, A. Petrou, O. Vakuliuk, T. Chatziioannou, I. Raptaki, S. Tsovola, I. Papakyriacou, A. Mitraki, D. T. Gryko and A. G. Coutsolelos, *Chem. Eur. J.* 2016, **22**, 11245.

S14 K. Kalyanasundaram, *Photochemistry and Photophysics of Polypyridine and Porphyrin Complexes*, Academic Press, London, 1996.

S15 T. Irebo, M.-T. Zhang, T. F. Markle, A. M. Scott and L. Hammarström, L. *J. Am. Chem. Soc.* 2012, **134**, 16247.

S16 A. Harriman, R. C. Richoux and P. Neta, *J. Phys. Chem.* 1983, **87**, 4957.

S17 Y. Pellegrin and F. Odobel, *C. R. Chimie* 2016, **20**, 283.

S18 C. Creutz, M. Chou, T. L. Netzel, M. Okumura and N. Sutin, *J. Am. Chem. Soc.* 1980, **102**, 1309.

S19 M. T. Indelli, C. Chiorboli, M. Ghirotti, M. Orlandi, F. Scandola, H. J. Kim and H.-J. Kim, *J. Phys. Chem. B* 2010, **114**, 14273.

S20 J. J. Warren, T. A. Tronic and J. M. Mayer, *Chem. Rev.* 2010, **110**, 6961.

S21 I. Kaljurand, A. Kütt, L. Soovali, T. Rodima, V. Maemets, I. Leito and I. A. Koppel, *J. Org. Chem.* 2005, **70**, 1019.

S22 J. Chen, M. Kuss-Petermann and O. S. Wenger, *Chem. Eur. J.* 2014, **20**, 4098.

S23 L. Biczòk, N. Gupta and H. Linschitz, *J. Am. Chem. Soc.* 1997, **119**, 12601.

S24 J. J. Concepcion, M. K. Brennaman, J. R. Deyton, N. V. Lebedeva, M. D. E. Forbes, J. M. Papanikolas and T. J. Meyer, *J. Am. Chem. Soc.* 2007, **129**, 6968.

S25 P. Dongare, A. G. Bonn, S. Maji and L. Hammarström, *J. Phys. Chem. C* 2017, **121**, 12569.

S26 J. Petersson and L. Hammarström, *J. Phys. Chem. B* 2015, **119**, 7531.